J Mater Sci (2018) 53:4874–4883

Chemical routes to materials

Fabrication of reduced graphene oxide decorated with gold and nickel for the catalytic reduction of 4-nitrophenol

Mingwei Cao[1,2], Lei Feng[1], Piaoping Yang[2,*], Hongxia Wang[1,*], Xu Liang[1], and Xiaowen Chen[1]

[1] Key Laboratory of Design and Synthesis of Functional Materials and Green Catalysis, College of Heilongjiang Province, Harbin Normal University, Harbin 150025, People's Republic of China

[2] College of Material Science and Chemical Engineering, Harbin Engineering University, Harbin 150001, People's Republic of China

Received: 10 August 2017
Accepted: 8 December 2017
Published online: 26 December 2017

ABSTRACT

Reduced graphene oxide (Ni/rGO) decorated by metallic Ni nanoparticles (NPs) was firstly fabricated through in situ thermal decomposition and subsequent reduction in 5% H_2/N_2 gas at 600 °C, and then Au NPs were loaded on the surface of the as-prepared Ni/rGO. X-ray diffraction (XRD), transmission electron microscopy (TEM), scanning electron microscope (SEM), X-ray photoelectron spectroscopy (XPS) and vibrating sample magnetometer (VSM) were used to characterize the Ni-decorated rGO and Ni/rGO@Au nanocomposites. The results show that both Ni and Au NPs are highly dispersed on rGO, and Ni/rGO@Au possesses excellent activity toward the conversion of 4-nitrophenol into 4-aminophenol in the presence of $NaBH_4$, showing almost four orders of magnitude higher activity parameter κ (9.7×10^{-2} $s^{-1}mg^{-1}$) than Ni/rGO (1.1×10^{-5} $s^{-1}mg^{-1}$), though Ni/rGO has a better performance in the catalytic conversion of 4-NP. In the meantime, the Ni/rGO@Au can be easily recycled by an external magnetic field and the conversion of 4-nitrophenol at the 8th cycle is still close to 95%.

Introduction

Au nanocatalysts have attracted considerable attention in the past three decades due to the abnormal catalytic activities at nanoscale compared with the inertness of bulk Au [1, 2]. However, aggregation is always a problem to be solved. Supporting Au nanocatalysts on moderate support can not only suppress the aggregation, improving the dispersion of Au nanoparticles (NPs), but also can reduce the loading of Au, cutting down the cost of preparation correspondingly.

Graphene, as an emerging two-dimensional material for loading metallic nanocatalysts, and its derivatives, graphene oxide (GO) and reduced graphene oxide (rGO) as well, are gaining increasing

Address correspondence to E-mail: yangpiaoping@hrbeu.edu.cn; hsdwanghx@yahoo.com

https://doi.org/10.1007/s10853-017-1913-9

attention due to the large specific surface area, abundant oxygen functional groups on the surface, excellent mechanical properties as well as better electronic conductivity [3–9]. Researches on Au nanocatalysts supported on graphene-based materials have been investigated intensively [7–10]. Among these researches, graphene materials are not just support materials, and they also participate in the electron transfer, promoting the conversion of reactant. By contrast, reduced graphene oxide (rGO) is more attractive as support materials due to better electronic conductivity [11, 12].

Therefore, we selected graphene oxide as basic support material to fabricate Ni-decorated rGO using in situ thermal decomposition and reduction method in this study and then decomposed Au NPs on amino-modified Ni/rGO. Though rGO/Ni nanocomposite has been synthesized previously by using GO and $NiCl_2{\cdot}6H_2O$ as raw materials in the presence of hydrazine hydrate or $NaBH_4$ [3, 13], the conversion time of 4-NP into 4-AP by the rGO/Ni seems too long, lasting for 140 and 180 min, respectively. Therefore, investigation on how to enhance the catalytic activity of Ni/rGO is necessary. Post-loading of Au NPs on Ni-decorated rGO is expected to improve the catalytic activity further since the catalytic activity of Au nanocatalyst is usually much better than that of non-noble metal catalyst. Sun et al. [14] synthesized a series of Au nanocatalysts by varying Au loading on tannic acid-treated graphene oxide and found that the conversion of 4-nitrophenol by some Au/GO nanocatalysts in the presence of $NaBH_4$ could be completed in a few minutes. In the study of Ma et al. [15], 1.5 nm Au NPs were successfully formed on thiophenol-modified graphene sheets, and the reduction of 4-nitrophenol (4-NP) by the as-prepared Au/TP-GS was very fast. This is also the best graphene-based monometallic Au nanocatalyst that has been reported so far for catalyzing the reduction of 4-NP in the presence of $NaBH_4$ except Au–Cu alloy nanoparticles attached on reduced graphene oxide [10]. In the present study, Ni-decorated rGO was first fabricated with a new method, followed by amino-modification, and then deposition of Au NPs on Ni-decorated rGO was carried out. The results indicate that the conversion of 4-NP into 4-AP by the Ni-decorated rGO is greatly accelerated in comparison with previous results [3, 13], and more remarkable improvement on the catalytic conversion of 4-NP is obtained after Au loading. In the meantime, the presence of Ni makes it easy to separate the as-prepared Ni/rGO@Au catalyst from liquid reaction system by using an external magnetic field.

Experimental

Materials

Nickel chloride, ammonium chloride, high-purity graphite flakes (> 99.99%), potassium permanganate ($KMnO_4$), sulfuric acid (H_2SO_4, 98%), hydrogen peroxide (H_2O_2, 30%), and ethanol (C_2H_5OH, 99.9%), sodium borohydride ($NaBH_4$, 99%), chloroauric acid ($HAuCl_4$, 99%) and 4-nitrophenol (4-NP) were all purchased from Sinopharm Chemical Reagent Co., Ltd (China). 3-Aminopropyltrimethoxysilane (APTES) was purchased from Sigma-Aldrich. All other chemicals were of analytical grade and used without further purification.

Synthesis of GO

Graphene oxide (GO) was first synthesized by the modified Hummers' method [16]. Firstly, 1 g of graphite was added into 23 mL of concentrated sulfuric acid (98%) under ice-water bath and stirred for 0.5 h and then 6 g of potassium permanganate was slowly added and kept stirring for another 2 h. Then, the mixture was transferred into a water bath under stirring, the temperature was firstly controlled at 40 °C for 0.5 h and then 140 ml of distilled water was added slowly at 80 °C. Finally, 60 mL of distilled water and 10.80 mL of H_2O_2 (30%) were added dropwise, and the color of the solution turned from dark brown to yellow. Thus, graphene oxide (GO) was obtained and separated by centrifugation after being washed with deionized water.

Synthesis of Ni/rGO nanocatalyst

The product was synthesized by an in situ thermal decomposition and reduction method. First, nickel chloride (0.75 mmol) and ammonia chloride (10 mmol) were dissolved in deionized water (20 mL) to form a clear solution. Next, 1 mL of ammonia solution (25%) was added to the solution slowly under stirring, during which the solution turned from green to blue immediately and was

denoted as "solution A." Then, 50 mL of the as-prepared GO solution (2 mg/mL) that was treated with ultrasound in advance for 10 min was added into solution A and kept stirring for another 10 min. Finally, the mixed solution was transferred into an autoclave, tightly sealed and heated at 100 °C for 12 h. The product was collected by centrifugation and washed with distilled water and absolute ethanol after the autoclave was cooled down to room temperature, and then was dried at 60 °C for 12 h, followed by heating at 600 °C in 5% H_2/N_2 gas for 3 h. The final product was denoted as Ni/rGO, where "rGO" means "reduced graphene oxide."

Synthesis of Ni/rGO@Au nanocatalyst

In order to anchor Au NPs stably, the Ni/rGO nanocomposite was modified with APTES in advance. Firstly, 20 mL of isopropanol solution containing 30 mg of the as-prepared Ni/rGO nanocomposite was ultrasonicated for 10 min, and then 400 μL of APTES was added into the suspension under mechanical stirring for 2 h at 80 °C. After magnetic separation and washing with isopropanol for three times, the amino-modified Ni/rGO nanocomposites were dispersed in a 20 mL of aqueous solution containing 10^{-3} M $HAuCl_4$ and 2.5×10^{-4} M trisodium citrate and kept stirring for 1 h. Then, 600 μL of freshly prepared 0.1M $NaBH_4$ solution was added into the solution under vigorous stirring, and the color of the solution turned to purple immediately, indicating the formation of Au NPs. After being heated at 60 °C for another 1 h, the product was washed and separated with a magnet, followed by drying at 40 °C in vacuum for 8 h and denoted as Ni/rGO@Au. In order to demonstrate the effect of APTES on the loading of Au nanoparticles, the loading of Au nanoparticles alone on graphene oxide with and without APTES modification beforehand was also performed. The modification of graphene oxide with APTES was carried out at 80 °C. The decomposition of Au NPs on graphene oxide is performed at room temperature.

Catalytic reduction of 4-nitrophenol (4-NP)

The reduction of 4-NP by $NaBH_4$ was chosen as a typical reaction to examine the catalytic activity of the Ni/rGO@Au nanocomposite. Distilled water (2 mL), aqueous solutions of 4-NP (60 μL, 5 mM) and $NaBH_4$ (0.5 mL, 0.2M) were mixed in a quartz curette without stirring. The color of the solution turned to bright yellow immediately after $NaBH_4$ was added. Then, the Ni/rGO@Au aqueous suspension (3 mg/mL, 30 μL) was injected into the solution without stirring. The reaction was monitored on a TU-1901 UV–vis spectrophotometer at a regular time interval of 30 s through its absorption peak at 400 nm [3, 9, 13] in the scanning range of 250–500 nm at room temperature. For comparison, Ni/rGO aqueous suspension with the same content (3 mg/mL, 30 μL) was also used for testing the reduction of 4-NP. In order to investigate the reusability of the as-prepared Ni/rGO@Au catalyst, the reduction reaction was magnified 20 times. In each cycle, the Ni/rGO@Au catalyst was separated by an external magnetic field after reaction and washed with water for the next cycle of catalysis. This procedure was repeated eight times.

Characterization

X-ray diffraction (XRD) measurement was examined on a Rigaku D/max-TTR-III diffractometer using monochromatic Cu Kα radiation ($\lambda = 0.15405$ nm). Transmission electron microscopy (TEM) and high-resolution transmission electron microscopy (HRTEM) micrographs were performed on an FEI Tecnai G2 S-Twin transmission electron microscope with a field emission gun operating at 200 kV. The morphologies of the GO were inspected on a scanning electron microscope (SEM, Hitachi S-4800). X-ray photoelectron spectroscopy (XPS) analysis was carried out on a Kratos Axis Ultra DLD spectrometer equipped with a monochromatic Al Kα X-ray source (1486.6 eV). Magnetization measurements were performed on a vibrating sample magnetometer (VSM, Lake-shore 7410) at room temperature.

Results and discussion

XRD patterns of the as-prepared GO, Ni/rGO and Ni/rGO@Au nanocomposites are shown in Fig. 1. The peak at $2\theta = 11.6°$ corresponds to carbon (002) of GO [17], and the broad peak at $2\theta = 25°$ corresponds to carbon (002) of rGO (Fig. S1) [17, 18]. The three diffraction peaks centering at 44.5°, 51.8°, and 76.4° are indexed to the reflections of the (111), (200), and (220) crystalline planes of cubic-phased Ni (JCPDS No. 04-0850), respectively. Different from Ni/rGO,

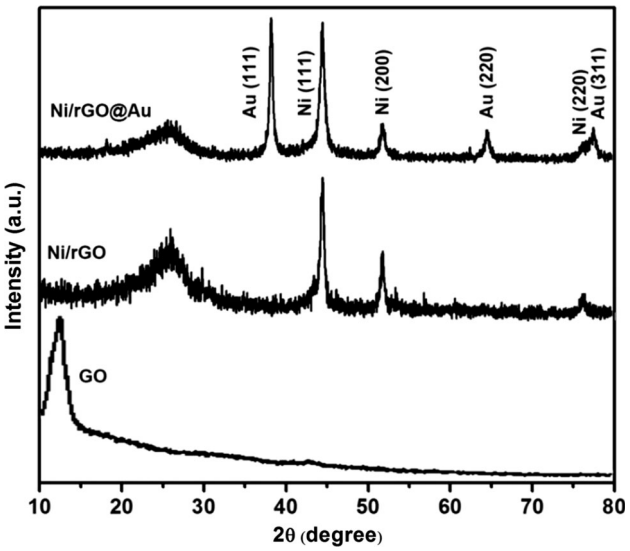

Figure 1 XRD patterns of GO, Ni/rGO and Ni/rGO@Au.

three new peaks ascribed to (111), (220) and (311) planes of cubic Au (JCPDS No. 04-0784) are observed in the diffraction pattern of Ni/rGO@Au. The sharpness of the peaks shows that both Au and Ni NPs attached on the surface of rGO have better crystallinity. In the meantime, the post-loading of Au on the surface of rGO has little effect on the crystallinity of Ni. Based on the Scherrer equation, the average crystallite size of Ni and Au NPs was calculated to be 9.2 and 4.6 nm, respectively, which is basically in agreement with the TEM analysis shown in Fig. S2.

Figure 2 shows the TEM images of Ni/rGO taken at low-magnification and high-magnification, respectively. Because GO exhibits a sheet-like morphology as shown in Fig. S3, it can be clearly seen in Fig. 2 that there are numerous sphere-like nanoparticles with high dispersion formed on graphene that was confirmed to be rGO by the XPS data listed below (Fig. 4). In the high-resolution TEM image (Fig. 2d), the distance between adjacent lattice fringes (marked by the arrows) of the nanoparticles is determined to be 0.203 nm, which corresponds to the d_{111} spacing of cubic Ni (JCPDS No. 04-0850). The selected area electron diffraction (SAED) pattern shown in the inset of Fig. 2d also displays three concentric rings corresponding to the (111), (200) and (220) crystalline planes of cubic nickel. These results demonstrate that the Ni-decorated rGO with highly dispersed Ni NPs on the surface of rGO was formed by using in situ thermal decomposition and reduction method.

Different from the TEM images of Ni/rGO, the particle size in the TEM images of Ni/rGO@Au is not uniform any more, and some smaller particles appears. Based on the EDS and mapping results shown in Fig. 3d, e, those smaller particles should be Au NPs, and the co-existence of Au and Ni NPs on rGO are confirmed by two different interplanar spacing (0.24 and 0.203 nm) shown in Fig. 3c, where the interplanar spacing of 0.24 nm corresponds to the (111) crystalline planes of Au NPs (JCPDS No. 04-0784). The mapping images also demonstrate that smaller Au NPs are highly dispersed on the surface of Ni/rGO.

Figure 4 shows the X-ray photoelectron spectroscopy (XPS) spectra of Ni/rGO@Au nanocatalyst. In the C 1s XPS spectrum, four peaks are distinguished after deconvolution and they are assigned to C–C (284.8 eV), C–O (286.8 eV), C=O (287.7 eV) and O–C=O (288.8 eV) [5, 6, 18], respectively. Compared with the C 1s XPS spectrum of GO shown in Ref. [5], the C 1s XPS spectrum in this study is more like that of rGO [5, 18, 19], since the peak for C–C are absolutely dominated in the spectrum in comparison with other peaks, like C–O and C=O [5, 20], which indicates considerable reduction of GO. The contribution from metallic nickel with Ni2p peak at 853 eV [5, 21–23] is very small and almost remains at the noise level. However, the XRD pattern shown in Fig. 1 confirms the existence of Ni NPs on the surface of rGO. We infer the absence of Ni2p signal in XPS spectrum might be caused by a lower Ni content in this area. The clear Au $4f_{7/2}$ and Au $4f_{5/2}$ doublets with binding energies of 83.3 and 86.8 eV are very close to the values of zero-valent Au [20, 24–27], which confirms the formation of Au NPs on Ni-decorated rGO.

In order to quantify the magnetism and find out whether the loading of Au NPs would bring serious decay to the magnetism of Ni/rGO, the magnetic hysteresis loops of the two samples were measured at room temperature. The saturated magnetizations (Ms) of the Ni/rGO were determined to be 4.8 emu/g and that of Ni/rGO@Au was 3.7 emu/g. Despite the lower Ms of Ni/rGO@Au, it is enough to recycle the catalyst from liquid reaction system by an external magnetic field as shown in the inset of Fig. 5. The lower Ms should be the result of a decrease in Ni relative content on the surface of rGO after Au

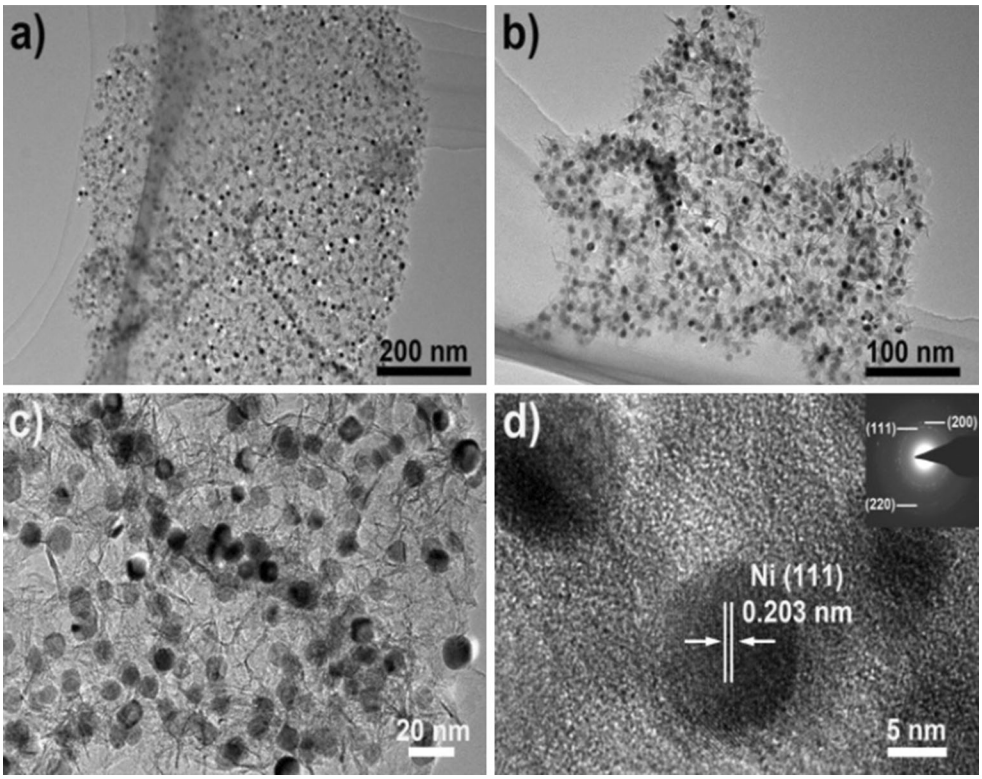

Figure 2 TEM images of Ni/rGO at **a**–**c** low-magnification and **d** high-magnification (inset is the SAED pattern).

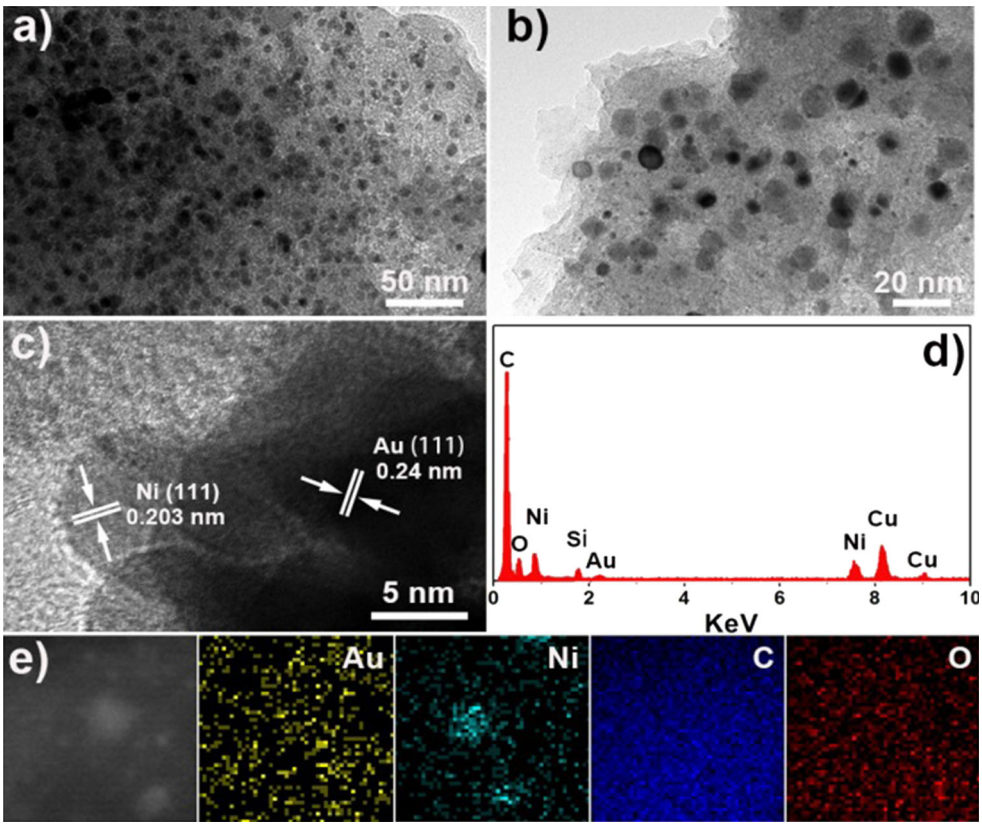

Figure 3 Images of Ni/rGO@Au nanocatalyst: **a**, **b** TEM Images, **c** HRTEM image, **d** EDS and **e** elemental mapping images.

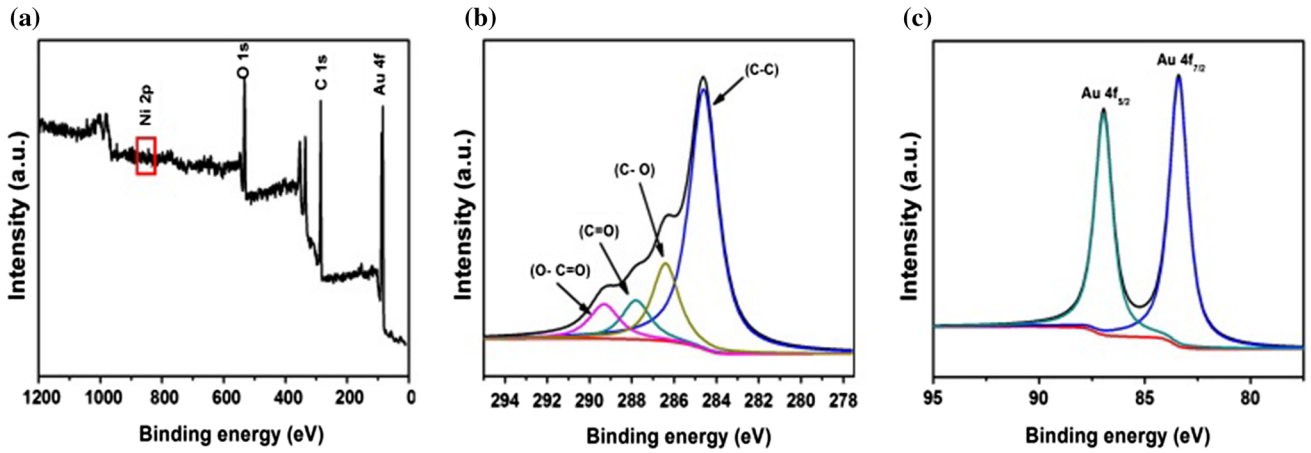

Figure 4 XPS spectra of Ni/rGO@Au nanocatalyst, **a** full survey, **b** C 1s, **c** Au4f.

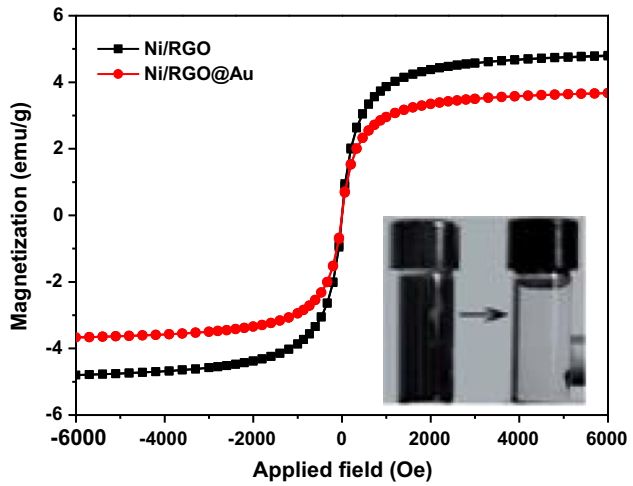

Figure 5 Magnetization curves of Ni/rGO@Au and Ni/rGO, the inset is a photograph of the Ni/rGO@Au sample before and after being separated by an external magnetic field.

loading. Moreover, the nearly zero remanence or coercivity of Ni/rGO@Au suggests a quasi-superparamagnetic nature [28–30], which is favorable for its dispersion in liquid medium.

Figure 6 shows the catalytic performance of Ni/rGO@Au and Ni/rGO toward the reduction of 4-NP in the presence of $NaBH_4$. In Fig. 6a, the absorbance band of 4-nitrophenolate at 400 nm generated due to the addition of $NaBH_4$ significantly decreases under the catalysis of Ni/rGO@Au nanocomposite (3 mg/mL, 30 μL) and almost disappears in 450 s [28, 29], in the meantime, a new peak with the center at 295 nm that is ascribed to 4-AP increases quickly, indicating a fast conversion of 4-NP into 4-AP. By contrast, the catalytic conversion of 4-NP by $NaBH_4$ in the presence of Ni/rGO is much slow. However, it is still much faster than that reported in Ref. [3, 13]. This demonstrates that the catalytic activity of Ni/rGO nanocomposite toward the reduction of 4-NP is improved greatly in comparison with that described in Ref. [3, 13]. Linear relationship between $\ln(C_t/C_0)$ and the reaction time for the reduction of 4-NP are shown in Fig. 6b and Fig. 6d, respectively. The results indicate that the conversion of 4-NP into 4-AP by $NaBH_4$ in the presence of Ni/rGO@Au and Ni/rGO in the present study matches well with the first-order reaction kinetics [29, 31], and the corresponding rate constant k is calculated to be 8.73×10^{-3} s^{-1} for Ni/rGO@Au and 0.067×10^{-3} min^{-1} for Ni/rGO@Au, respectively.

To further investigate the stability of the Ni/rGO@Au nanocomposite for the reduction of 4-NP, the nanocomposite was reused for several times and the result are shown in Fig. 7. It can be seen that the conversion of 4-NP by $NaBH_4$ in the Ni/rGO@Au catalyst only has a slight decrease after eight consecutive cycles, with a 95% conversion at the 8th cycle. ICP data demonstrates a very slight decrease in the amount of Ni and Au on the surface of rGO after eight consecutive cycles for reducing 4-NP (Table S1). Because trace amount of solids was noticed in supernatant during separation by an external magnetic field, the slight decrease in the conversion of 4-NP during consecutive cycles is very possibly the result of the loss of trace amount of Ni/rGO@Au rather than the deactivation of the catalyst, demonstrating a better stability of Ni/rGO@Au catalyst or better resistance to deactivation.

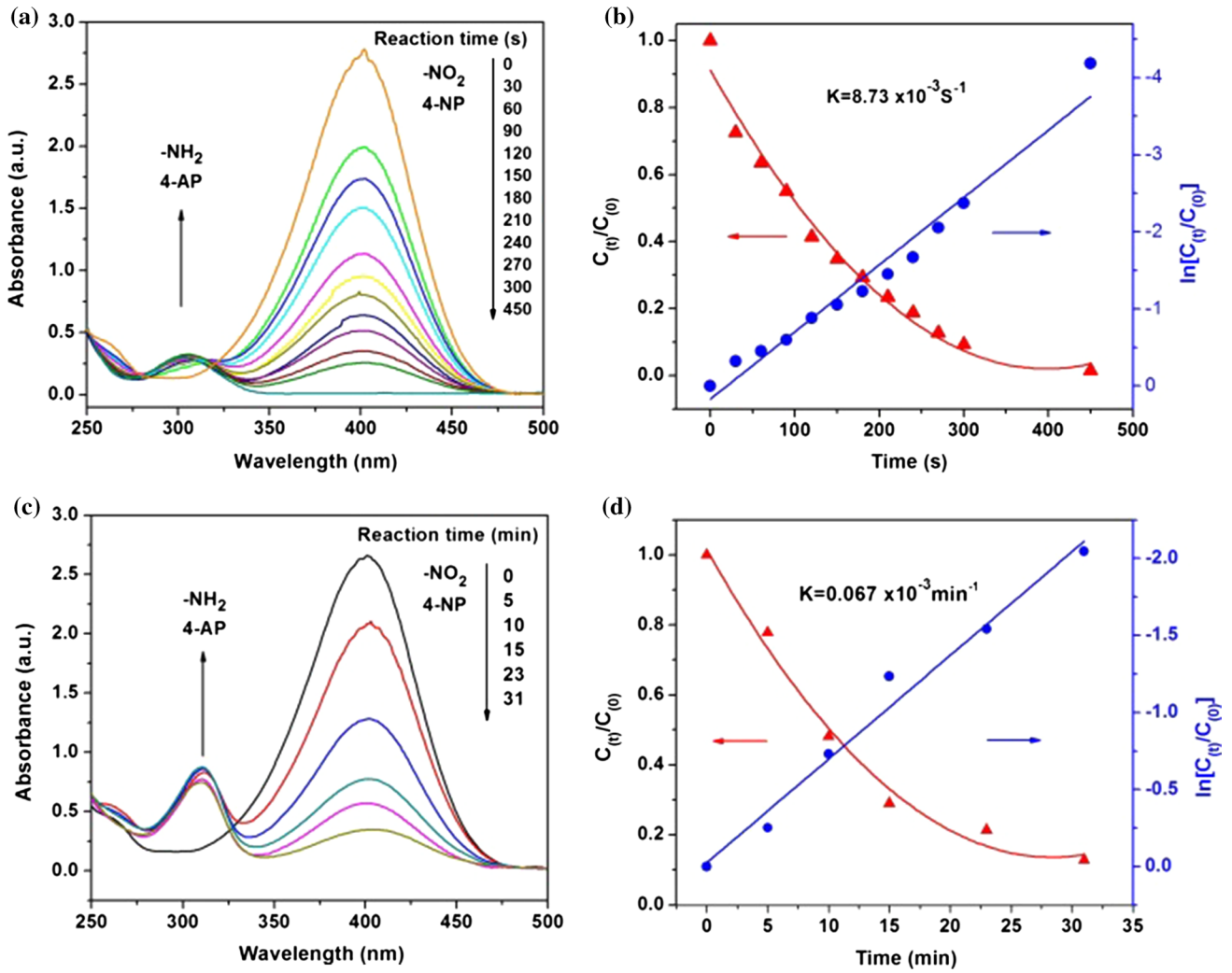

Figure 6 UV–Vis absorption spectra of 4-AP and 4-NP before and after adding $NaBH_4$, as well as C_t/C_0 and $\ln(C_t/C_0)$ versus reaction time for the reduction of 4-NP by $NaBH_4$ in the presence of **a**, **b** Ni/rGO@Au and **c**, **d** Ni/rGO.

As the rate constant k is generally determined by the preparation methods, support materials, the amount of catalyst and so on [3, 28, 32], activity parameter κ that is defined as the ratio of rate constant (k) to the loading amounts of catalyst [28, 33, 34] is also calculated in the present study in order to evaluate the catalytic activity of catalyst more reasonably. The activity parameter κ for Ni/rGO@Au and Ni/rGO is 9.7×10^{-2} and 1.1×10^{-5} s^{-1} mg^{-1}, respectively. Obviously, the catalytic activity of Ni/rGO@Au is much higher than that of the Ni/rGO, almost four orders of magnitude higher than that of Ni/rGO. In addition, we noticed that the rate constant k of Ni/rGO@Au in the present study is slightly lower than that reported in the Ref. [15], which is also the best result on monometallic Au nanocatalyst supported on graphene for catalytic conversion of 4-NP to 4-AP. In the study by Ma et al. [15] the 4-aminothiophenol was used to modify the graphene before Au loading, and the rate constant k of the resultant Au nanocatalyst toward the reduction of 4-NP to 4-AP is 9.39×10^{-3} s^{-1}. In the present study, the surface of the Ni-decorated rGO was reacted with APTES before Au loading. As a result, the rate constant k of the resultant Au nanocatalyst toward the reduction of 4-NP to 4-AP is 8.73×10^{-3} s^{-1}. We infer the difference in rate constant is related to the different functional groups on support surface, –SH and $–NH_2$, which leads to different particle size of Au NPs and different catalytic activity. It is well known

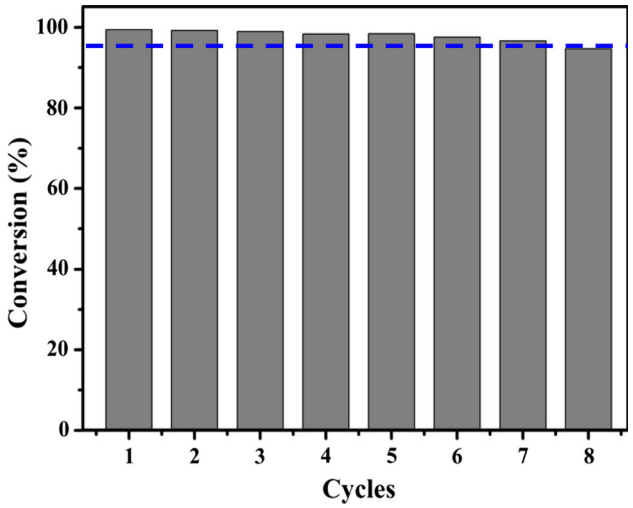

Figure 7 The reusability of Ni/rGO@Au catalyst for the reduction of 4-NP by $NaBH_4$.

that –SH groups has higher affinity to Au than $–NH_2$ and –COOH groups. The binding strength varies in the order of Au–S > Au–NH_2 > Au–COOH [35, 36]. So, it is rational to get Au nanoparticles with smaller particle size on –SH-modified graphene than on –NH_2- or –COOH-modified graphene due to the different affinity between Au and functional groups on graphene. Here, we mainly modified Ni/rGO with APTES before Au loading, expecting a more homogeneous dispersion of Au NPs with smaller particle size to be formed on Ni/rGO. Fig. S4 clearly shows that the particle size of Au nanoparticles formed on graphene oxide became smaller after the graphene was modified with APTES. However, the particle size is still bigger than that reported by Ma et al. [15]. Then, why does the Ni/rGO@Au catalyst have a similar rate constant to that with smaller Au NPs on graphene [15]? We infer that the better catalytic activity of the as-prepared Ni/rGO@Au nanocatalyst in the present study has a close relationship with the perfect dispersion of Ni and Au NPs on the surface of rGO as well as their synergetic catalysis toward the reduction of 4-NP. Both Au and Ni NPs have the ability to catalyze the reduction of 4-NP into 4-AP in the presence of $NaBH_4$, and the better dispersion of Ni and Au NPs on graphene can ensure that there are more catalytic active sites to be exposed to reactant. In the meantime, the synergetic catalysis of Ni and Au NPs provides Ni/rGO@Au catalyst with better stability together with their better dispersion on graphene oxide.

Conclusions

In summary, loading Au nanoparticles on Ni-decorated rGO is satisfying in getting a highly efficient Ni/rGO@Au catalyst for the reduction of 4-NP. First, Ni-decorated rGO was prepared using in situ thermal decomposition and reduction in 5% H_2/N_2 flow at 600 °C by using GO and $NiCl_2$ as raw materials. Highly dispersed Ni NPs were formed on the surface of rGO, and the time for the conversion of 4-NP by $NaBH_4$ in the presence of the as-prepared Ni/rGO is greatly shortened. Second, Au nanoparticles with high distribution were in situ anchored to amino-modified Ni/rGO using $NaBH_4$ as reducing agent, and the activity parameter κ of the Ni/rGO@Au catalyst is almost four orders of magnitude higher than that of Ni/rGO. Third, the as-prepared Ni/rGO/Au nanocatalyst with the characteristic of easy separation has better stability or better resistance to catalyst deactivation and therefore can be reused for many times without obvious decrease in the conversion of 4-NP into 4-AP.

Acknowledgements

The authors gratefully acknowledge financial support from the National Natural Science Foundation of China (NSFC 21271053, 21401032, 51472058), Natural Science Foundation of Heilongjiang Province (B201403), Scientific Research foundation for the Returned Overseas Chinese Scholars, Education Department of Heilongjiang Province (LC2016002).

Electronic supplementary material: The online version of this article (https://doi.org/10.1007/s10853-017-1913-9) contains supplementary material, which is available to authorized users.

References

[1] Hvolbæk B, Janssens TVW, Clausen BS, Falsig H, Christensen CH, Nørskov JK (2007) Catalytic activity of Au nanoparticles. Nanotoday 2:14–18

[2] Rao CNR, Kulkarni GU, Thomas PJ, Edwards PP (2002) Size-dependent chemistry: properties of nanocrystals. Chem Eur J 8:28–35

[3] Ji Z, Shen X, Zhu G, Zhou H, Yuan A (2012) Reduced graphene oxide/nickel nanocomposites: facile synthesis, magnetic and catalytic properties. J Mater Chem 22:3471–3477

[4] Wu Sh, He Q, Zhou Ch, Qi X, Huang X, Yin Z, Yang Y, Zhang H (2012) Synthesis of Fe_3O_4 and Pt nanoparticles on reduced graphene oxide and their use as a recyclable catalyst. Nanoscale 4:2478–2483

[5] She Y, Lu Z, Fan W, Jewell S, Leung MKH (2014) Facile preparation of PdNi/rGO and its electrocatalytic performance towards formic acid oxidation. J Mater Chem A 2:3894–3898

[6] Guo Y, Sun X, Liu Y, Wang W, Qiu H, Gao J (2012) One pot preparation of reduced graphene oxide (RGO) or Au(Ag) nanoparticle-RGO hybrids using chitosan as a reducing and stabilizing agent and their use in methanol electrooxidation. Carbon 50:2513–2523

[7] Atar N, Eren T, Demirdögen B, Yola ML, Çağlayan MO (2015) Silver, gold, and silver@gold nanoparticle-anchored L-cysteine-functionalized reduced graphene oxide as electrocatalyst for methanol oxidation. Ionics 21:2285–2293

[8] Ghosh S, Holade Y, Remita H, Servat K, Beaunier P, Hagège Kokoh KB, Napporn TW (2016) One-pot synthesis of reduced graphene oxide supported gold-based nanomaterials as robust nanocatalysts for glucose electrooxidation. Electrochim Acta 212:864–875

[9] Gupta VK, Atar N, Yola ML, Üstündağ Z, Uzun L (2014) A novel magnetic Fe@Au core–shell nanoparticles anchored graphene oxide recyclable nanocatalyst for the reduction of nitrophenol compounds. Water Res 48:210–217

[10] Rout L, Kumar A, Dhaka RS, Reddy GN, Giri S, Dash P (2017) Bimetallic Au–Cu alloy nanoparticles on reduced graphene oxide support: synthesis, catalytic activity and investigation of synergistic effect by DFT analysis. Appl Catal A 538:107–122

[11] Stankovich S, Dikin D, Dommett G, Kohlhaas K, Zimney E, Stach E, Piner R, Nguyen S, Ruoff R (2006) Graphene-based composite materials. Nature 442:282–286

[12] Li D, Kaner RB (2008) Graphene-based materials. Science 320:1170–1171

[13] Chen G, Wang F, Liu F, Zhang X (2014) One-pot preparation of Ni-graphene hybrids with enhanced catalytic performance. Appl Surf Sci 316:568–574

[14] Zhang Y, Liu S, Lu W, Wang L, Tian J, Sun X (2011) In situ green synthesis of Au nanostructures on graphene oxide and their application for catalytic reduction of 4-nitrophenol. Catal Sci Technol 1:1142–1144

[15] Ren R, Li S, Li J, Ma J, Liu H, Ma J (2015) Enhanced catalytic activity of Au nanoparticles self-assembled on thiophenol functionalized graphene. Catal Sci Technol 5:2149–2156

[16] William S, Jr Hummers, Offeman RE (1958) Preparation of graphitic oxide. J Am Chem Soc 80:1339

[17] Li L, Gao P, Gai S, He F, Chen Y, Zhang M, Yang P (2016) Ultra small and highly dispersed Fe_3O_4 nanoparticles anchored on reduced graphene for supercapacitor application. Electrochim Acta 190:566–573

[18] Zheng H, Yang S, Zhao J, Zhang Z (2014) Synthesis of rGO–Ag nanoparticles for high-performance SERS and the adsorption geometry of 2-mercaptobenzimidazole on Ag surface. Appl Phys A 114:801–808

[19] Barman BK, Nanda KK (2015) Rapid reduction of GO by hydrogen spill-over mechanism by in situ generated nanoparticles at room temperature and their catalytic performance towards 4-nitrophenol reduction and ethanol oxidation. Appl Catal A 491:45–51

[20] Johra F, Jung W (2016) Low temperature synthesis of RGO-Au nanocomposite with apparently reduced time and its application as a chemical sensor. Appl Surf Sci 362:169–175

[21] Prieto P, Nistor V, Nouneh K, Oyama M, Abd-Lefdil M, Díaz R (2012) XPS study of silver, nickel and bimetallic silver–nickel nanoparticles prepared by seed-mediated growth. Appl Surf Sci 258:8807–8813

[22] Zhang G, Li W, Xie K, Yu F, Huang H (2013) A one-step and binder-free method to fabricate hierarchical nickel-based supercapacitor electrodes with excellent performance. Adv Funct Mater 23:3675–3681

[23] Niu L, Wang J, Hong W, Sun J, Fan Z, Ye X, Wang H, Yang S (2014) Solvothermal synthesis of Ni/reduced graphene oxide composites as electrode material for supercapacitors. Electrochim Acta 123:560–568

[24] Wu Y, Zhang T, Zheng Z, Ding X, Peng Y (2010) A facile approach to Fe_3O_4@Au nanoparticles with magnetic recyclable catalytic properties. Mater Res Bull 45:513–517

[25] Atar N, Eren T, Yola ML, Karimi-Maleh H, Demirdögen B (2015) Magnetic iron oxide and iron oxide@gold nanoparticle anchored nitrogen and sulfur-functionalized reduced graphene oxide electrocatalyst for methanol oxidation. RSC Adv 5:26402–26409

[26] Xia Q, Fu S, Ren G, Chai F, Jiang J, Qu F (2016) Fabrication of Fe_3O_4@Au hollow spheres with recyclable and efficient catalytic properties. New J Chem 40:818–824

[27] Liang S, Xia Y, Zhua S, Zheng S, He Y, Bi J, Liu M, Wu L (2015) Au and Pt co-loaded g-C_3N_4 nanosheets for enhanced photocatalytic hydrogen production under visible light irradiation. Appl Surf Sci 358:304–312

[28] Niu Z, Zhang S, Sun Y, Gai S, He F, Dai Y, Li L, Yang P (2014) Controllable synthesis of Ni/SiO_2 hollow spheres and

their excellent catalytic performance in 4-nitrophenol reduction. Dalton Trans 43:16911–16918

[29] Pan W, Zhang S, He F, Gai S, Sun Y, Yang P (2015) A cheap and efficient catalyst with ultra-high activity for reduction of 4-nitrophenol. CrystEngComm 17:5744–5750

[30] Yeh C, Chen D (2014) Ni/reduced graphene oxide nanocomposite as a magnetically recoverable catalyst with near infrared photothermally enhanced activity. Appl Catal B 150–151:298–304

[31] Ayán VM, Fernández MMJ, Paredes JI, Villar RS, Fernández SC, Guardia L, Martínez AA, Tascón JMD (2014) Highly efficient silver-assisted reduction of graphene oxide dispersions at room temperature: mechanism, and catalytic and electrochemical performance of the resulting hybrids. J Mater Chem A 2:7295–7305

[32] Jiang Z, Xie J, Jiang D, Wei X, Chen M (2013) Modifiers-assisted formation of nickel nanoparticles and their catalytic application to p-nitrophenol reduction. CrystEngComm 15:560–569

[33] Rocha M, Fernandes C, Pereira C, Rebelo SLH, Pereira MFR, Freire C (2015) Gold-supported magnetically recyclable nanocatalysts: a sustainable solution for the reduction of 4-nitrophenol in water. RSC Adv 5:5131–5141

[34] An Q, Yu M, Zhang Y, Ma W, Guo J, Wang C (2012) Fe_3O_4@Carbon Microsphere Supported Ag–Au bimetallic nanocrystals with the enhanced catalytic activity and selectivity for the reduction of nitroaromatic compounds. J Phys Chem C 116:22432–22440

[35] Chen F, Li X, Hihath J, Huang Z, Tao N (2016) Effect of anchoring groups on single-molecule conductance: comparative study of thiol-amine-, and carboxylic-acid-terminated molecules. J Am Chem Soc 128:15874–15881

[36] Hong W, Manrique DZ, Moreno-García P, Gulcur M, Mishchenko A, Lambert CJ, Bryce MR, Wandlowski T (2012) Single molecular conductance of tolanes: experimental and theoretical study on the junction evolution dependent on the anchoring group. J Am Chem Soc 134:2292–2304